BIOCHEMISTRY
including biophysical chemistry & molecular biology

Article

pubs.acs.org/biochemistry

Structure-Based Alteration of Substrate Specificity and Catalytic Activity of Sulfite Oxidase from Sulfite Oxidation to Nitrate Reduction

James A. Qiu,[†] Heather L. Wilson, and K. V. Rajagopalan*

Department of Biochemistry, Duke University Medical Center, Durham, North Carolina 27710, United States

ABSTRACT: Eukaryotic sulfite oxidase is a dimeric protein that contains the molybdenum cofactor and catalyzes the metabolically essential conversion of sulfite to sulfate as the terminal step in the metabolism of cysteine and methionine. Nitrate reductase is an evolutionarily related molybdoprotein in lower organisms that is essential for growth on nitrate. In this study, we describe human and chicken sulfite oxidase variants in which the active site has been modified to alter substrate specificity and activity from sulfite oxidation to nitrate reduction. On the basis of sequence alignments and the known crystal structure of chicken sulfite oxidase, two residues are conserved in nitrate reductases that align with residues in the active site of sulfite oxidase. On the basis of the crystal structure of yeast nitrate reductase, both positions were mutated in human sulfite oxidase and chicken sulfite oxidase. The resulting double-mutant variants demonstrated a marked decrease in sulfite oxidase activity but gained nitrate reductase activity. An additional methionine residue in the active site was proposed to be important in nitrate catalysis, and therefore, the triple variant was also produced. The nitrate reducing ability of the human sulfite oxidase triple mutant was nearly 3-fold greater than that of the double mutant. To obtain detailed structural data for the active site of these variants, we introduced the analogous mutations into chicken sulfite oxidase to perform crystallographic analysis. The crystal structures of the Mo domains of the double and triple mutants were determined to 2.4 and 2.1 Å resolution, respectively.

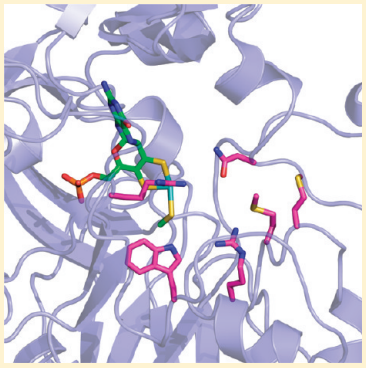

Sulfite oxidase (SO)[1] is a member of the family of proteins containing the molybdenum cofactor (Moco) that consists of a single Mo atom coordinated through a dithiolene group to molybdopterin (MPT).[2] The Mo atom is coordinated to the protein via a single cysteine residue.[3] Eukaryotic SO is an essential protein that resides in the intermembrane space of the mitochondria and catalyzes the essential oxidation of sulfite to sulfate in the terminal step of the degradation of sulfur-containing compounds, including the amino acids methionine and cysteine. Loss of the ability to oxidize sulfite can be due to either a defect in the Moco biosynthetic pathway or point mutations in the *sox* gene itself.[4] Of the human enzymes containing Moco, only SO is essential, and a number of point mutations in the SO gene have been previously identified in SO-deficient patients.[5] SO deficiency leads to severe effects, including seizures, attenuated brain growth, mental retardation, and other neurological and metabolic problems, usually resulting in death during the first year of life.[6] The sulfite oxidation reaction catalyzed by SO is in eq 1, and a scheme of the likely reaction cycle is provided in Figure 1.[7]

$$SO_3^{2-} + H_2O + 2(cytc)_{ox} \rightarrow SO_4^{2-} + 2(cytc)_{red} + 2H^+ \quad (1)$$

In the first part of the cycle (reductive half-reaction), sulfite binds at the Mo^{VI} center and is oxidized to sulfate, generating a two-electron-reduced $Mo^{IV}Fe^{III}$ species.[8] In the first intramolecular electron transfer (Figure 1, IET #1) between the Mo and heme domains, one of the two reducing equivalents generated by sulfite oxidation is transferred from Mo^{IV} to the b_5-type heme in the N-terminal domain, yielding a transient $Mo^{V}Fe^{II}$ species. The second part of the cycle (oxidative half-reaction) begins with the transfer of an electron from the heme to the exogenous

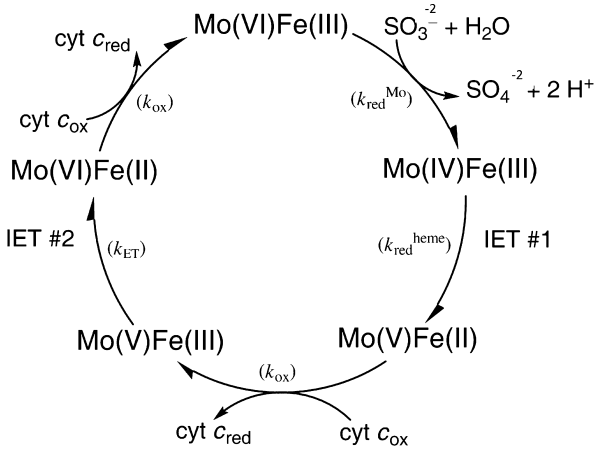

Figure 1. Reaction cycle of SO.

Received: August 3, 2011
Revised: January 19, 2012
Published: January 20, 2012

   dx.doi.org/10.1021/bi201206v | *Biochemistry* 2012, 51, 1134–1147

electron acceptor, cytochrome *c* (cyt *c*). After a second IET from Mo^{V} to Fe^{III}, the fully oxidized species is regenerated by the transfer of an electron from Fe^{II} to a second molecule of cyt *c*. Eukaryotic SO is purified as a homodimer of ~52 kDa subunits, and each subunit consists of an N-terminal b_5-type heme domain, a central domain containing the Moco, and a C-terminal region mediating dimerization[9,10] (Figure 2).

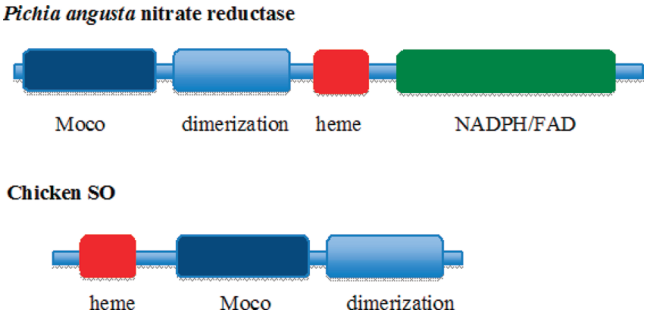

Figure 2. Domain structure of SO and NR proteins. The monomer of *Pichia angusta* NR is arranged with an N-terminal Moco domain, a dimerization domain, a heme domain, and a NADPH/FAD domain. In comparison, the CSO monomer contains an N-terminal heme domain, a central Moco domain, and a C-terminal dimerization domain.

Structure of Chicken SO. The crystal structure of chicken liver SO was determined at a resolution of 1.9 Å[11] (Figure 3A). The structure revealed a sulfate molecule bound in the active site, allowing identification of the likely ligands and H-bonds to the substrate during catalysis. The coordination around the Mo atom in the active site consists of two oxo groups (equatorial and axial) and three sulfur ligands, including two dithiolene sulfurs and the thiol group of Cys 185 arranged in a square pyramidal geometry.[12] Solvent gains access via a positively charged channel that opens onto the equatorial oxo group of the Mo atom. The substrate binding pocket is positively charged and is formed by five residues, including three arginines at positions 138, 190, and 450, Tyr 322, and Trp 204. All five of these residues are conserved in all eukaryotic SO proteins isolated to date. The importance of Arg 138 and 190 (Arg 160 and 211, respectively, in human SO) was demonstrated by the identification of the R160Q and R211Q mutations in human patients presenting with severe SO deficiency.[11] The structural and kinetic characterization of the R160Q variant has been accomplished using a variety of techniques, including flash photolysis[13] and EXAFS.[14] Very recently, the molybdenum site of this clinical mutant was investigated by a combination of X-ray absorption spectroscopy and density functional theory calculations.[14] On the basis of these studies, this variant has a six-coordinate pseudo-octahedral active site with coordination of the Oε atom of Gln 160 to molybdenum.[14] This is in contrast to the wild-type SO active site that is five-coordinate and exhibits approximately square-based pyramidal geometry.[15] While mutations of the remaining substrate binding pocket residues have yet to be observed in human patients, the Tyr 322 (Tyr 343 in human SO) residue was proposed to be important in labilizing the oxo group of Mo^{VI} to allow the transfer of oxygen to sulfite based on the proximity of this residue to the equatorial oxo group in the crystal structure. Furthermore, this residue has been proposed to serve an additional role as a proton shuttle between water (or OH) in the coupled electron−proton transfer (CEPT) mechanism during reduction and reoxidation of the

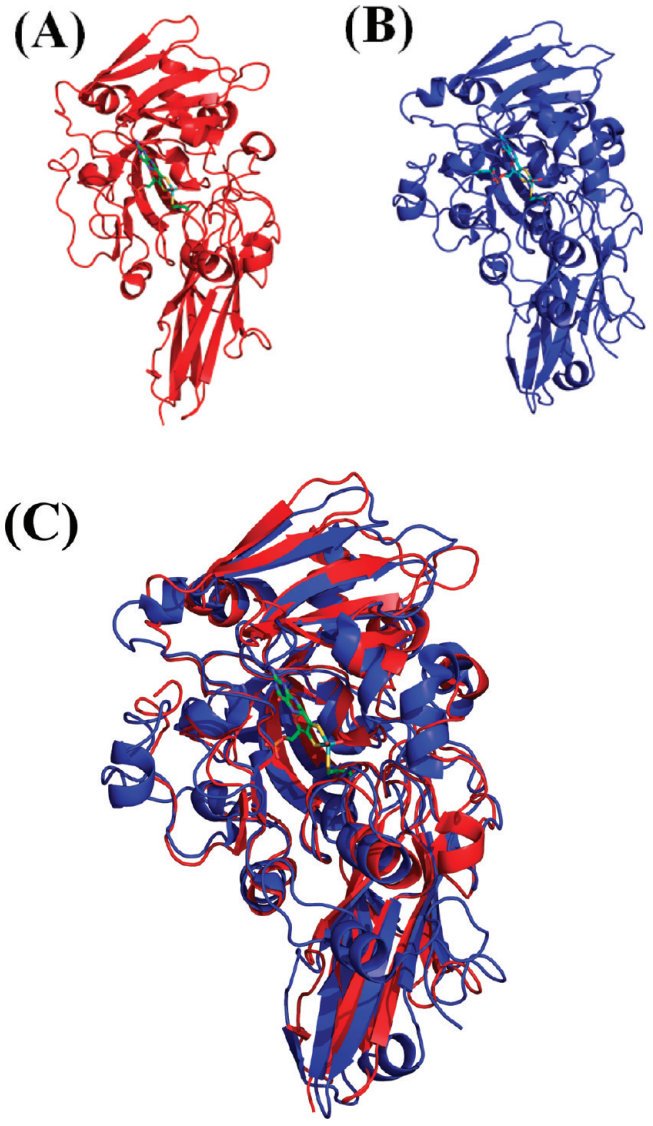

Figure 3. Model of active sites of SO/NR with substrates. Structures of the Mo domains of (A) sulfite oxidase and (B) nitrate reductase. (C) Alignment of chicken SO (red) and the *P. angusta* NR (blue) Mo domains showed excellent agreement. The Moco is shown as green sticks.

Mo center.[16] The human Y343F variant has been created, and extensive kinetic and structural studies have indicated that the Tyr residue is critical for substrate binding,[17] IET,[18] and overall catalysis, including serving as a proton shuttle between the Mo−oxo group and water (or hydroxo) in the coupled electron−proton transfer during reduction and reoxidation of the Mo center.

Structure of Plant SO. In 2003, the structure of a second member of the SO superfamily, *Arabidopsis thaliana* SO, was determined at a resolution of 2.3 Å.[19] Plant SO is homodimeric but is devoid of the heme domain. In contrast to chicken SO, plant SO crystallized without a sulfate bound in the active site. While the five active site residues mentioned above are strictly conserved between mammalian and plant SO, only four of them superimposed with the residues in the chicken SO active site. The exception was Arg 374 (equivalent to Arg 450 and 472 in chicken and human SO, respectively), in which the side

dx.doi.org/10.1021/bi201206v | *Biochemistry* 2012, 51, 1134−1147

chain pointed toward the solvent access channel rather than toward the bound sulfate seen in the chicken SO structure. Because there was no sulfate in the active site, on the basis of these findings, Arg 374 was proposed to be essential for both substrate recruitment and binding and specificity because of its conformational change in the presence of bound substrate.

Structure of Recombinant Chicken SO. Because SO is the only Moco-containing protein essential for normal human development, structure−function studies of the enzyme are of significant relevance to human health. Unfortunately, human SO (sequence 68% identical to that of chicken SO) remains resistant to crystallization, and the gene for chicken SO has never been isolated; therefore, there are significant barriers to performing structure−function studies on mammalian SO or in determining disease etiology in mutants isolated from human patients with SO deficiency. However, recently, our lab successfully created an artificial gene for chicken SO, allowing us to successfully introduce mutations into the chicken SO protein to begin structure−function studies.[20] When recombinant chicken SO was crystallized in both sulfate-bound and unbound conformations, this represented the first time the same Moco enzyme was crystallized in the presence and absence of the product, and later in the presence and absence of substrate,[12] verifying that the Arg 450 (human Arg 472) residue does indeed change conformation depending on the presence of substrate in the active site.[17] The Arg 450 residue pointed toward the active site in the presence of substrate, coordinating the sulfite, but when no sulfite was present, the side chain pointed toward the solvent access channel. This change in conformation results in a much smaller binding pocket and shifts the position of the sulfur away from the Mo atom, presumably preparing the pocket for product release and possibly transmitting conformational changes to other parts of the protein, including the heme domain, allowing domain movement to occur during the reaction cycle. It should be noted that Arg 450 is located in the dimerization domain, so it has also been proposed that this residue could possibly transmit conformational changes from the active site to the dimer interface, thus transmitting information between the two subunits of SO. However, until now, the importance of this third active site Arg in either substrate binding or activity had never been directly verified by site-directed mutagenesis or kinetic analysis. In this study, we changed the Arg 472 residue in human SO (analogous to Arg 450 in chicken SO) to either Met or Gln to directly observe changes in the activity of the protein as a result of the change at this position from a positive to an uncharged residue.

R138Q Variant of Chicken SO. The de novo creation of the chicken SO gene also allowed the structure of the R138Q chicken SO protein to be determined.[20] As predicted from previous work on the analogous R160Q human protein,[13] the replacement of a positively charged arginine with a neutral glutamine in the active site changed the surface potential of the active site and solvent access channel; however, this change was not due only to the loss of the positive charge of Arg 138. The most significant structural change in the active site of the R138Q mutant was actually the orientation of the side chain of Arg 450 toward the active site due to the loss of the repulsive effect of the Arg 138 side chain on Arg 450 in the absence of sulfate in the active site. This resulted in a significant change in the position of the Arg 450 (Arg 472 in humans and Arg 374 in plants) residue, resulting in negative charges becoming exposed along the solvent access tunnel so that despite the absence of sulfate in the active site, the side chain of Arg 450 was pointing into the active site, creating a much smaller binding pocket. Thus, this residue was found to occupy a position similar to that in a wild-type product-occupied pocket, albeit in the absence of product.

Assimilatory Nitrate Reductase (NR). Assimilatory NR is a member of the SO family of Moco-containing enzymes that catalyzes the first step of nitrate assimilation in algae, fungi, and plants.[21−23] Assimilatory NR forms homodimers of approximately 120 kDa, and oligomerization is dependent upon MPT. NR catalyzes the overall reaction

$$NO_3^- + NAD(P)H \rightarrow NO_2^- + NAD(P) + OH^- \quad (2)$$

The reaction cycle of NR begins with the reductive half-reaction when NAD(P)H reduces FAD. The second step is IET via heme as in SO. The third step is the oxidative half-reaction in which Mo transfers two electrons to nitrate, which serves as both the terminal two-electron acceptor and as the substrate, yielding the reaction products nitrite and a hydroxyl ion.[24] While NR and SO perform opposite reactions on their respective substrates, there is 31% identity between the heme domains of chicken SO and assimilatory NR from *Arabidopsis thaliana* and 38% between their respective Mo domains,[11] and in both cases, the electron flow is from the C-terminus to the N-terminus of the multidomain protein (Figure 2). The X-ray structure of the Mo domain of *Pichia angusta* NR was recently determined to 1.7 Å.[25] The structure of the Moco in NR is identical to that found in chicken SO (Figure 3B), and four of the six active site residues are conserved. The two variant residues are Tyr 322 and Arg 450 of SO, which are replaced by Asn and Met/Leu or Val, respectively. In all NR sequences, the Asn residue corresponding to the Tyr in SO is strictly conserved. There appears to be a division over the consensus sequence of the residue corresponding to Arg 450 in SO between the lower eukaryotic fungal NRs and higher eukaryotic plant NRs. A Met, Leu, or Thr replaces Arg 450 of chicken SO at the analogous position in fungal NRs, whereas in all plant NRs, the Arg is replaced with Met. Given the difference in substrates (NO_3^- vs SO_3^{2-}), it is proposed that Arg 450 is replaced because nitrate has to be bound with one of its O atoms positioned toward the Mo atom for subsequent removal to produce the nitrite product. Stopped-flow kinetic analysis of the plant NR revealed that the overall catalytic rate was not limited by any individual step, and unlike SO, the transfer of electrons between domains appeared to be rate-limiting in NR because the rate was much faster when an artificial electron donor such as methyl viologen or bromphenol blue was used rather than an NAD(P)H-driven reaction.[24]

Rational Design of SO Variants with NR Activity. Enzyme specificity toward substrates is determined in part by the local encoding of a complementary surface to a given substrate by the active site residues.[26] The following work describes the strategy by which the substrate specificity and activity of SO enzymes have been altered. Using predictions from the sequence alignments of SO and NR and analysis of the crystal structures of chicken SO and the NR Mo domain from *P. angusta* (Figure 3C), the predicted catalytic site residues of NR were introduced into chicken and human SO. We designed and characterized several SO variants. The resulting variants were assayed for their ability to oxidize sulfite to sulfate and for the acquisition of nitrate reduction. The double mutant was less able to oxidize sulfite and more able to

reduce nitrate. Additionally, a third position in NR was identified near the edge of the active site that was hypothesized to play a role in substrate binding. This additional position was introduced into both double mutants to generate SO triple variants. The triple mutants of both human SO and chicken SO exhibited a higher affinity for nitrate and moderately enhanced NR activity compared to that of the double mutants.

Finally, we were able to crystallize chicken SO nitrate reductase variants CSO-2NR and CSO-3NR, determining the structures to 2.4 and 2.1 Å resolution, respectively, yielding detailed structural information about the active sites of these variants. The creation of these variant proteins has provided unique insights into the varying functions of these two Moco-containing proteins. This information should be particularly valuable in understanding more about the nitrate reductase active site, as these proteins are generally less amenable to characterization than are sulfite oxidase proteins.

EXPERIMENTAL PROCEDURES

Site-Directed Mutagenesis of Eukaryotic SO Enzymes. All mutations in human SO that have been described were directly introduced into the pTG918 plasmid[27] using the Transformer site-directed mutagenesis kit as previously described (Clontech Laboratories Inc., Mountain View, CA).[17,20] The CSO-2NR variant was generated in wild-type CSO expression vector pTRC99a CLSO.2 with the R161G background. The Y322N mutation was introduced by overlapping primer extension polymerase chain reaction.[28] The R450M mutation was introduced using the Transformer site directed mutagenesis kit as described above. The CSO-3NR variant Y322N, R450M, and V452M mutations were introduced into the pTRC99a CLSO.2 vector as described above. All resulting constructs were verified by sequencing at the Duke University DNA analysis facility.

Expression and Purification of SO. All recombinant forms of SO were expressed in the TP1000 strain of *Escherichia coli* and purified as previously described.[18,27] For gel-filtration analysis of the oligomeric state of SO variants, purified protein (at 1 mg/mL) was injected onto a Superdex-200 FPLC column equilibrated with 50 mM potassium phosphate buffer and eluted using a flow rate of 1 mL/min. The FPLC system consisted of an AKTA Explorer system, and protein was monitored at 280 nm. The concentration of purified SO was determined from the A_{413} using an extinction coefficient of 113 mM^{-1} cm^{-1}.

Molybdenum Analysis. The Mo content of protein samples was quantified by atomic absorption spectroscopy using a Spectra AA-220 double-beam atomic absorption spectrometer (Varian, Palo Alto, CA). Subsequent analyses were conducted using the conditions described previously by Johnson.[3,29]

Sulfite Oxidase Activity Assays. Steady-state kinetic assays were performed aerobically at 25 °C using a 1.0 cm path length cuvette in a Shimadzu UV-1601PC spectrophotometer. Assays were conducted in 20 or 50 mM buffers adjusted to the desired pH with acetic acid to minimize anion inhibition of SO as previously described.[8,17] The following buffers were used: Bis-Tris (pH 6.0−6.5), Bis-Tris propane (pH 6.5−7.5), Tris (pH 7.5−8.5), and glycine (pH 9.0−10.0). The glycine buffers were adjusted to the desired pH using NaOH. Steady-state pH profiles were obtained using 15−50 μM horse heart cyt *c* (Sigma), 0.50−2.5 μg/mL SO, and varying concentrations of sulfite in a final assay volume of 1 mL. The reduction of cyt *c* was monitored at 550 nm using an extinction coefficient of 19 mM^{-1} cm^{-1}. The steady-state reaction parameters k_{cat} and K_m were obtained by a direct fit of the concentration dependence to the Michaelis−Menten equation using Kaleidagraph (Synergy Software). Steady-state assays with ferricyanide as the electron acceptor were performed using 20 mM buffers as described above, 40 μM ferricyanide, 1.5−5.0 μg/mL SO, and varying concentrations of sulfite in a final assay volume of 1 mL. The reduction of ferricyanide was monitored at 420 nm, and enzyme activity is reported in units per milligram, where one unit is equal to an absorbance change of 1.0 AU/min at 420 nm.

Nitrate Reductase Assays. Nitrate reductase assays were conducted anaerobically at 25 °C using dithionite-reduced methyl viologen as the electron donor and monitoring the oxidation of MV at 600 nm using a Shimadzu UV-1601PC spectrophotometer. Nitrate reductase assays were conducted anaerobically at 25 °C using dithionite-reduced methyl viologen (MV) as the electron donor and monitoring its oxidation at 600 nm using an extinction coefficient of 8.25 mM^{-1} cm^{-1}.[30] Assay conditions include 20 μM MV, 50 μg of enzyme, and varying concentrations of potassium nitrate in a final volume of 2 mL. Measurement of nitrate reductase activity was conducted at pH 7.0 using 50 mM Bis-Tris propane and at pH 8.5 using 50 mM Tris-HCl. The pH of the buffer was adjusted with acetic acid to minimize anion inhibition. The change in absorption was monitored on a Shimadzu UV-1601PC spectrophotometer. All buffer solutions were made anaerobic by being bubbled with argon gas for at least 30 min prior to use. All assays were prepared in an anaerobic chamber (Coy Laboratory Products Inc., Grass Lake, MI) in 13 mm × 100 mm cuvettes and sealed with a rubber septum. The assay reagents methyl viologen, sodium dithionite, and potassium nitrate were brought into the anaerobic chamber as dry stocks, and solutions were prepared using anaerobic buffer. The steady-state reaction parameters k_{cat} and K_m were obtained by a direct fit of the concentration dependence to the kinetic studies.

Stopped-Flow Assays of HSO. Rapid reaction kinetic studies were performed using an SX.20MV stopped-flow reaction analyzer (Applied Photophysics Ltd.) as previously described.[8,17] The dead time of the instrument was determined to be <1.5 ms with a path length of 10 mm. To prepare the instrument for anaerobic operation, the sample tubing and valve lines were incubated with 250 mM sodium dithionite for several hours and then thoroughly rinsed with O_2-free water. Additionally, the sample-handling unit of the stopped-flow apparatus was fitted with an anaerobic accessory that enclosed the drive syringe plungers and was continuously flushed with nitrogen gas. The reaction temperature was maintained at 25 °C using a circulating water bath connected to the thermostat bath housing the drive syringes. All solutions were made anaerobic by being bubbled with argon gas for at least 30 min prior to use, and solutions of human SO were prepared by diluting <100 μg of a concentrated stock of the enzyme into a final volume of ∼5 mL of anaerobic buffer. All dilutions were performed in an anaerobic chamber (Coy Laboratory Products Inc.), and 5 mL Hamilton gastight syringes were used to load samples into the stopped-flow spectrophotometer. Rapid kinetic assays of the reductive half-reaction were performed anaerobically at 25 °C using 0.3−0.8 μM protein. Reduction of the SO b_5-type heme was directly monitored by measuring the extinction change of the Soret peak at 425 or 430 nm. The k_{obs} of each individual reaction was obtained by fitting individual kinetic traces to single- or double-exponential curves

dx.doi.org/10.1021/bi201206v | *Biochemistry* 2012, 51, 1134−1147

using a nonlinear least-squares Levenberg−Marquardt algorithm. The maximal rate parameter k_{red} and the $K_d^{sulfite}$ for the reductive half-reactions were obtained by fitting the k_{obs} at varying sulfite concentrations to a hyperbolic curve as shown below.

$$k_{obs} = k_{red}[S]/(K_d + [S]) \quad (3)$$

Crystallization of the Nitrate Reductase Variants of CSO. After purification, the CSO-2NR variant was buffer exchanged using a PD-10 ion exchange column (GE Healthcare) into 20 mM Tris (pH 7.8) and 100 mM NaCl and concentrated to 25 mg/mL using a Vivaspin 30000 concentrator (Vivascience). This sample served as a stock protein solution and was stored at 4 °C prior to crystallization. From this stock solution, the protein was diluted to a 10 mg/mL solution using a buffer solution of 20 mM Tris (pH 7.8) containing 100 mM NaCl. Crystals of the CSO-2NR variant were obtained by the hanging drop vapor diffusion method at 17 °C, by adding 2 μL of protein solution to 2 μL of crystallization solution equilibrated against 1 mL of reservoir crystallization solution of 17% PEG 10000 (w/v), 10 mM barium chloride dihydrate, 100 mM ammonium acetate, and 100 mM Bis-Tris propane (pH 5.5). Red crystals were observed after 3 weeks and were grown for 5−6 weeks. Crystals were transferred to the crystallization solution containing 5% glycerol, the level of which was increased stepwise to a final concentration of 30%, and then flash-frozen in liquid nitrogen. The crystals grew in space group $I4_1$ with a solvent content of 54.5% and the following unit cell dimensions: a = 85.62 Å, b = 85.62 Å, and c = 153.37 Å. The CSO-3NR variant crystal form was grown under crystallization conditions consisting of 15% (w/v) PEG 6000, 5% (v/v) MPD, 100 mM MES (pH 6.5), and 2% (w/v) benzamidine hydrochloride hydrate by the hanging drop method as described above. The crystals were observed after 3 weeks, reaching a final size by 6 weeks, were red in color, and grew in space group $I4_1$ with a solvent content of 54.3% and the following unit cell dimensions: a = 85.6 Å, b = 85.6 Å, and c = 152.8 Å.

X-ray diffraction data sets were collected for both the CSO-2NR and CSO-3NR variants at the South East Regional Collaborative Access Team (SER-CAT) BM-22 line at the Advanced Photon Source, Argonne National Laboratory (Argonne, IL). All data sets were scaled and indexed using DENZO and SCALEPACK.[31] The structures were determined by molecular replacement using PHASER in the CCP4 suite of programs. The coordinates from recombinant chicken SO residues 95−466 [Protein Data Bank (PDB) entry 2A99] excluding the cofactor and solvent molecules were used for the molecular replacement search model.[32] Iterative model building using COOT[33] with PROBE[34] for visualization of all-atom contacts and refinement was done with REFMAC.[35] The stereochemistry of the structures was evaluated using MOLPROBITY[36] to assess the Ramachandran plots and atomic clash scores. For the structures reported in this study, TLS refinement was performed at the final stages of refinement,[37] and water molecules were added to complete the models using COOT.

RESULTS AND DISCUSSION

HSO R472Q and R472M Single-Substitution Variants. When the crystal structure of plant SO was determined, all residues in the active site superimposed with the previously determined chicken SO structure with the exception of the side chain of the Arg 374 residue (analogous to Arg 450 and 472 in chicken and human SO, respectively). Because plant SO crystallized in the absence of sulfate, it was proposed that this residue plays a crucial role in substrate recruitment and binding.[19] To directly test the role of this residue in substrate binding, we generated and purified the R472Q (for a similarly sized but uncharged substitution) and R472M (the analogous residue in NR) variants of human SO. Both variants behaved like wild-type SO during purification and were purified as dimers with a full complement of Mo as measured by atomic absorption spectroscopy.

Somewhat surprisingly, steady-state kinetics of both of these variants indicated that substitution at this position had very little effect on the $K_m^{sulfite}$, and even at high pH, the values were very comparable to those of wild-type SO (Table 1). In contrast to the $K_m^{sulfite}$ values, both mutations had drastic effects on catalysis as measured by the ability to reduce the exogenous electron acceptor cyt c in the presence of sulfite (Table 2). The impairment of catalysis was particularly pronounced at high pH values.

Table 1. $K_m^{sulfite}$ for Wild-Type SO and Its R472Q and R472M Variants[a]

pH	wild-type K_m (μM)	R472Q K_m (μM)	R472M K_m (μM)
6.0	1.29	2.32	1.95
7.0	2.72	3.51	2.45
8.0	4.35	13.0	4.72
8.5	8.25	16.2	9.38
9.0	22.1	45.3	21.2
9.5	67.1	96.7	53.7
10.0	52.9	181.7	96.9

[a]Steady-state assays were conducted aerobically as described in Experimental Procedures.

Table 2. k_{cat} Values for Wild-Type SO and Its R472Q and R472M Variants[a]

pH	wild-type k_{cat} (s^{-1})	R472Q k_{cat} (s^{-1})	R472M k_{cat} (s^{-1})
6.0	13.2	8.17	5.02
7.0	24.2	5.77	3.60
8.0	25.9	9.34	3.48
8.5	26.9	4.58	3.77
9.0	25.7	4.24	3.44
9.5	26.3	1.67	1.81
10.0	13.0	0.52	0.46

[a]Steady-state assays were conducted aerobically as described in Experimental Procedures.

Stopped-Flow Analysis of the Reductive Half-Reaction of R472Q and R472M. Stopped-flow analysis of wild-type, R472Q, and R472M SO was performed in the absence of cyt c by measuring the spectral change in the Soret peak at 425 nm allowing direct observation of the reduction of heme during the reductive half-reaction and obtaining a rate for IET #1 (Figure 1). In contrast to the k_{cat} values described above, the k_{red} values for both of these proteins were quite high at both pH 7.0 and 8.5 (Table 3). R472Q demonstrated nearly wild-type rates, and R472M had approximately values that 50% of the wild-type rates at both pH values. These results were somewhat unexpected because overall the level of catalysis in both of these proteins is less than 10% of that of the wild type (Table 2).

Table 3. Rapid Reaction Kinetics for Wild-Type, R472Q, and R472M SO[a]

	k_{red} (s^{-1})	$K_d^{sulfite}$ (μM)
pH 8.5		
wild type	82.8	6.72
R472Q	71.2	227
R472M	38.9	73.4
pH 7.0		
wild type	70.2	2.05
R472Q	83.4	14.5
R472M	39.0	3.23

[a]Stopped-flow analysis was conducted anaerobically as described in Experimental Procedures.

Another surprising result was the high $K_d^{sulfite}$ at pH 8.5 for both proteins, particularly R472Q; this was not anticipated in view of the nearly wild-type $K_m^{sulfite}$ values obtained in the steady-state assays for both of these proteins (Table 1).

These results form a direct contrast to the reductive half-reaction rates obtained in our laboratory for previously analyzed active site variants, including R160Q[16] and Y343F.[17] For both of these proteins, we obtained very low k_{red} values at pH 8.5 (5.3 and 4.8 s^{-1} for R160Q and Y343F, respectively), as well as very high $K_d^{sulfite}$ values that were very close to the $K_m^{sulfite}$ values obtained for the steady-state reactions.

To rule out the possibility that the interaction of the heme domain with the exogenous electron acceptor cyt *c* was adversely affected in these variants, resulting in a low overall level of catalysis but high reductive half-reaction rates, steady-state kinetics were performed in which the concentration of sulfite was held constant and that of cyt *c* was varied. The $K_m^{cyt\ c}$ obtained for R742Q was 4 μM and for R472 M was 4.1 μM, which in both cases was very close to the wild-type value of 4.4 μM.

Mo domains of R472Q and R472M SO. To measure the ability of R472Q and R472M to oxidize sulfite and transfer electrons to an artificial electron acceptor in the absence of the heme domain, the R472Q and R472M mutations were created in the Mo domain of SO. As seen in the stopped-flow results described above, when the nonspecific electron acceptor ferricyanide (rather than cyt *c*) is used in steady-state assays, the V_{max} was not nearly as impaired as when cyt *c* was used for either protein (Table 4). Also similar to the stopped-flow

Table 4. Steady-State Activity of the Mo Domains of Wild-Type, R472Q, and R742M SO Using Ferricyanide as an Artificial Electron Acceptor

	V_{max} (units/mg)	$K_m^{sulfite}$ (μM)
pH 8.5		
wild type	99.8	14.9
R472Q	99.6	223
R472M	46.4	94.0
pH 7.0		
wild type	78.0	4.56
R472Q	50.5	12.8
R472M	27.9	5.00

results in which the K_d for both proteins significantly increased (Table 3), the $K_m^{sulfite}$ increased significantly in these assays, as well (Table 4).

Again, the R472Q and R472M Mo domain variants are different from other previously characterized human SO variants (e.g.,Y343F and R160Q), which have impaired catalysis, but also demonstrate a similarly weak ability to reduce a nonspecific electron acceptor such as ferricyanide.

Human SO Y343N/R472M (HSO-2NR) Variant. Of the five core residues forming the active site of SO, two are not conserved between SO and NR proteins. These two residues, Tyr 343 and Arg 472 (human numbering), were switched to the Asn and Met residues found in NR proteins. Upon examination of the single-substitution variant proteins at these two positions (Y343N and R472M), it is clear that these two residues play distinct roles. The Tyr 343 residue clearly plays an important role in mediating substrate specificity, because the Y343N single mutant demonstrates significant impairment of the ability to bind sulfite (Table 5) while retaining catalytic

Table 5. $K_m^{sulfite}$ Values of Active Site HSO Variants

pH	wild-type K_m (μM)	Y343N K_m (μM)	V474M K_m (μM)	Y343F/R472Q K_m (μM)	Y343N/R472M K_m (μM)	Y343N/R472M/V474M K_m (μM)
6.0	1.29	95.3	0.46	61.4	16800	1100
7.0	2.72	94.7	1.34	87.7	4640	1420
8.0	4.35	297	3.19	282.7	19280	2140
8.5	8.25	850	3.54	712.5	42990	14000
9.0	22.1	2460	14.4	3340	85640	55500
9.5	67.1	9370	31.9	39900	208000	111000
10.0	52.9	12013	40.2	59660	ND[a]	418000

[a]Not determined.

Table 6. k_{cat} Values of Active Site Mutants

pH	wild-type k_{cat} (s^{-1})	Y343N k_{cat} (s^{-1})	V474M k_{cat} (s^{-1})	Y343F/R472Q k_{cat} (s^{-1})	Y343N/R472M k_{cat} (s^{-1})	Y343N/R472M/V47M k_{cat} (s^{-1})
6.0	13.2	3.17	5.96	1.44	1.35	1.90
7.0	24.2	12.77	11.4	1.73	1.13	3.37
8.0	25.9	13.75	17.8	2.05	1.33	3.58
8.5	26.9	16.91	15.8	2.25	1.42	3.90
9.0	25.7	15.54	19.6	2.31	1.13	5.60
9.5	26.3	8.11	17.1	4.94	0.97	5.23
10.0	13.0	4.38	12.4	2.96	ND[a]	2.80

[a]Not determined.

activity [~60% of that of the wild type at pH 8.5 (Table 6)], while the R472M single mutant as discussed above has an essentially wild-type $K_m^{sulfite}$ but only ~10% of wild-type catalytic activity (Tables 1 and 2). The Y343N/R472M double mutant (HSO-2NR) behaved like wild-type HSO and was purified as a dimer.[10] The HSO-2NR variant lost essentially all ability to bind sulfite as demonstrated by a $K_m^{sulfite}$ of 42.9 mM at pH 8.5, 5000-fold higher than the wild-type value of 8.25 μM (Table 5). Furthermore, HSO-2NR was severely impaired in its ability to oxidize sulfite (Table 6) across the range of pH values measured, resulting in a second-order rate constant ($k_{cat}/K_m^{sulfate}$) 7 orders of magnitude below that of wild-type SO (Table 7). However, this protein gained the ability to bind nitrate with a $K_m^{nitrate}$ of 568 μM as demonstrated by methyl viologen-mediated nitrate reduction assays performed at pH 8.5, while wild-type SO has negligible ability to either bind or reduce nitrate (Table 8). While this initial result was encouraging, the measured $K_m^{nitrate}$ of 568 μM at pH 8.5 was approximately 10-fold higher than that observed in native NR proteins. However, when the assays were performed using

dx.doi.org/10.1021/bi201206v | *Biochemistry* 2012, 51, 1134–1147

Table 7. Second-Order Rate Constants ($k_{cat}/K_m^{sulfite}$) of Active Site Mutants

pH	wild type	Y343N	V474M	Y343F/R472Q	Y343N/R472M	Y343N/R472M/V474M
6.0	1.02×10^7	3330	1.30×10^6	2350	8.04	173
7.0	8.90×10^6	1.35×10^4	8.51×10^5	1970	24.4	237
8.0	5.95×10^6	4630	5.58×10^5	725	6.90	167
8.5	3.26×10^6	1990	4.46×10^5	316	3.30	27.9
9.0	1.16×10^6	632	1.36×10^5	69.2	1.32	10.1
9.5	3.92×10^5	86.6	5.36×10^4	12.4	0.47	4.71
10.0	2.46×10^5	36.5	3.08×10^4	4.96	ND[a]	0.67

[a]Not determined.

Table 8. Nitrate Reducing Activity of the HSO Variants and Wild-Type NR Proteins

	$K_m^{nitrate}$ (μM)	k_{cat} (s^{-1})	$k_{cat}/K_m^{nitrate}$ ($M^{-1}s^{-1}$)	ref
pH 8.5				
wild-type SO	43000	<0.10	ND[a]	this work
HSO-2NR	568	0.65	1.1×10^3	this work
HSO-3NR	192	0.67	3.5×10^3	this work
pH 7.0				
HSO-2NR	24	0.82	3.4×10^4	this work
HSO-3NR	30	1.07	3.5×10^4	this work
Spilanthes oleracea	12	180	1.5×10^7	39
A. thaliana	90	100	1.1×10^6	24
Pichia pastoris	30	159	5.3×10^6	38

[a]Not determined.

standard nitrate reductase conditions at pH 7.0, the value of 24 μM was well within the range of native NR proteins,[24,38,39] though the rate of catalysis remained quite low (Table 8).

Human SO Y343N/R472M/V474M (HSO-3NR) Variant. On the basis of sequence analysis, the importance of an additional Met residue found in the active site of all NR proteins rather than the Val residue found in that position in SO proteins was not obvious. However, on the basis of the recently determined crystal structure of yeast NR,[25] the Met residue found in the active site of NR was proposed to be important in catalysis of nitrate reduction, because the side chain of this residue changed conformation depending on the presence or absence of nitrate like Arg 472, which changes position in SO. Therefore, the homologous Val residue in SO was changed to a Met to create a triple-variant SO protein (Y343N/R472M/V474M). This triple mutant was expressed, and its behavior during purification was identical to that of wild-type HSO.[10] Interestingly, while the sulfite oxidation ability of this protein remained very weak as expected, it was less impaired than HSO-2NR particularly at higher pH values, with higher k_{cat} and lower $K_m^{sulfite}$ values at all pH values (Tables 5–7). When nitrate reductase assays were performed at pH 8.5, $K_m^{nitrate}$ decreased from 568 to 192 μM, and at pH 7.0, the k_{cat} increased slightly more than 2-fold, from 0.82 to 2.13 s^{-1} (Table 8)

Role of the Heme Domain in the NR Activity of HSO-2NR and HSO-3NR. Previous studies using the native NR Mo domain fragment have demonstrated that the heme domain and the FAD domain are not necessary for activity in the presence of a ready supply of electron donors such as reduced viologens.[38] Purification of the Mo domains of both HSO-2NR and -3NR allowed us to answer the question of whether the heme domain is necessary for nitrate reduction in this system (Table 9). The Mo

Table 9. Nitrate Reducing Activity of the Mo Domains of Human Wild-Type SO, HSO-2NR, and HSO-3NR

	$K_m^{nitrate}$ (μM)	k_{cat} (s^{-1})
pH 8.5		
SO Modom	2270	0.13
Mo HSO-2NR	872	0.47
Mo HSO-3NR	371	0.63
pH 7.0		
SO Modom	1410	0.06
Mo HSO-2NR	42	0.62
Mo HSO-3NR	37	1.93

fragments of both HSO-2NR and HSO-3NR retained low $K_m^{nitrate}$ values and k_{cat} values similar to those of full-length proteins (Table 8), demonstrating that the heme domain is not needed as long as there is a source of electrons from dithionite and reduced viologens.

Absorption Spectra of the Mo Domains of HSO-NR Variants. Generating the Mo domains of these variants in the absence of the heme domain also allowed us to measure absorption spectra and to visualize the Mo center in a way that is not possible in the presence of the strongly absorbing heme chromophore (Figure 4). While the spectrum of the single

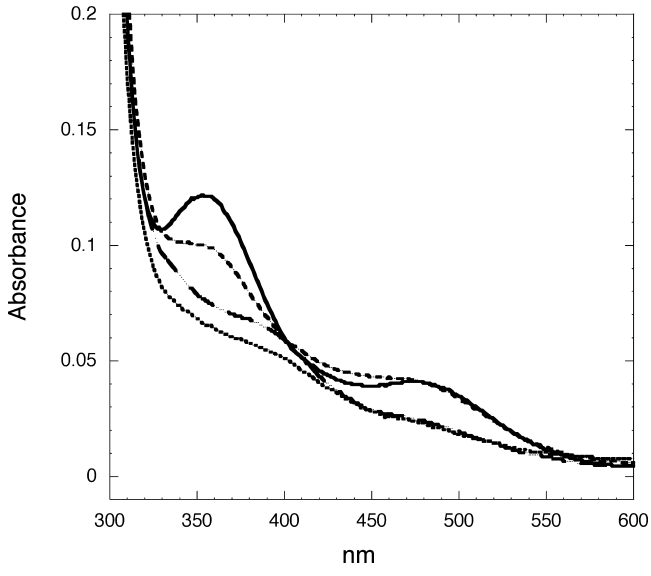

Figure 4. Absorption spectra of SO variants: (—) wild type, (···) Y343N, (–·–) SO-2NR, and (---) SO-3NR.

dx.doi.org/10.1021/bi201206v | Biochemistry 2012, 51, 1134–1147

active site mutants R472M and V474M appeared to be identical to that of the wild type (data not shown), absorption spectroscopy revealed significant differences in the 480 and 350 nm absorption bands for the Y343N variant (Figure 4), indicating altered geometry in the enedithiolate-to-Mo charge transfer band at 360 nm and in the Cys 207 to Mo charge transfer as demonstrated by a blue shift in the 480 nm band.

Chicken SO Y322F/R450M (2NR) Variant. In the crystal structure of chicken SO, the active site residue Arg 450 (equivalent to Arg 472 of HSO) was observed to change conformation depending on the presence of the sulfate. This suggested that Arg 450 was involved in substrate recruitment. Further examination of the crystal structure of the active site of chicken SO suggested that Tyr 322, because of its proximity to the molybdenum of the Moco, might play a role in electron transport and substrate recruitment (Figure 5). This

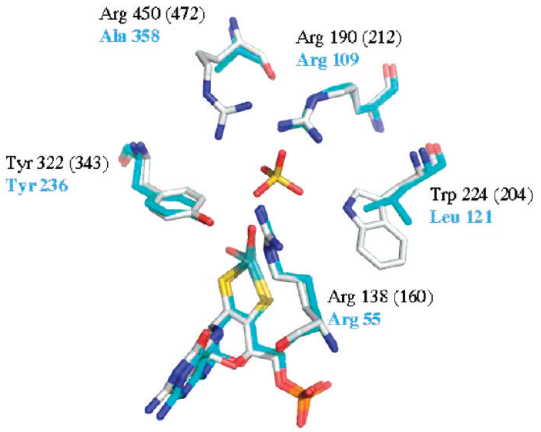

Figure 5. Overlay of chicken SO (black) and human SO (black in parentheses) with bacterial SDH (blue) active site residues.

supposition was supported by studies conducted with human SO variant Y343F.[17,18] When the Mo domain of assimilatory NR was crystallized, the active site was found to superimpose with the active site of SO at four of six positions.[25] Interestingly, the two positions that were not identical were Tyr 322 and Arg 450 of CSO, which are strongly conserved in all SO proteins. Tyr 322 corresponds to an Asn in NR, and Arg 450 corresponds to a Met in plant NRs or to a Leu/Thr in fungal NR proteins. This observation suggested that it might be possible to modulate the substrate affinity and convert the enzymatic activity of SO from sulfite oxidation to nitrate reduction. Because the HSO variants discussed above (HSO-2NR and HSO-3NR) were not amenable to crystallization, the equivalent double mutant of chicken SO, Y322N/R450M (CSO-2NR), was generated, cloned, expressed, and behaved like wild-type CSO during purification,[9] and was characterized for sulfite oxidase and nitrate reductase activity. The variant exhibited a markedly weakened ability to bind sulfite at pH 8.5 with a $K_m^{sulfite}$ of 11730 μM and a weakened ability to oxidize sulfite to sulfate with a $k_{cat}^{sulfite}$ of 2.52 s^{-1} for a second-order rate constant $k_{cat}/K_m^{sulfite}$ of 2.14×10^2 compared to wild-type CSO with a $K_m^{sulfite}$ of 8.43 μM and a $k_{cat}^{sulfite}$ of 73.3 s^{-1} for a $k_{cat}/K_m^{sulfite}$ of 8.69×10^6. At pH 7.0, the 2NR variant exhibited an improvement in the ability to bind sulfite with a $K_m^{sulfite}$ of 561 and an improved $k_{cat}^{sulfite}$ of 4.83 s^{-1} for a second-order rate constant of 8.61×10^3 that was still considerably lower than that of wild-type SO with a $K_m^{sulfite}$ of 1.28 μM and a $k_{cat}^{sulfite}$ of 35.9 s^{-1} for a $k_{cat}/K_m^{sulfite}$ of 8.69×10^7 (Table 10).

Table 10. Sulfite Oxidizing Activity of the CSO Variants and Wild-Type NR Proteins

	$K_m^{sulfite}$ (μM)	$k_{cat}^{sulfite}$ (s^{-1})	$k_{cat}/K_m^{sulfite}$ (M^{-1} s^{-1})	ref
pH 8.5				
CSO	8.43	73.3	8.7×10^6	20
CSO	8.53	71.4	8.3×10^6	this work
CSO-2NR	11730	2.52	2.1×10^2	this work
CSO-3NR	6750	4.1	6.1×10^2	this work
pH 7.0				
CSO	1.28	35.9	2.8×10^7	20
CSO	1.33	36.1	2.7×10^7	this work
CSO-2NR	561	4.83	8.6×10^3	this work
CSO-3NR	570	2.18	3.8×10^3	this work

When assayed for nitrate reduction activity at pH 8.5, wild-type CSO exhibited negligible ability to reduce or bind nitrate, whereas the CSO-2NR variant exhibited a $K_m^{nitrate}$ of 1134 μM and a $k_{cat}^{nitrate}$ of 0.751 s^{-1} for a $k_{cat}/K_m^{nitrate}$ of 6.62×10^2. When the 2NR variant was assayed under standard conditions at pH 7.0, the 2NR variant exhibited a $K_m^{nitrate}$ of 445 μM and a $k_{cat}^{nitrate}$ of 0.65 s^{-1} for a $k_{cat}/K_m^{nitrate}$ of 1.46×10^3. While it was encouraging to observe modified substrate affinity and catalytic activity from sulfite oxidation to nitrate reduction in CSO, the Michaelis constant values were much higher than that of native NR enzymes (Table 11).

Table 11. Nitrate Reducing Activity of the CSO Variants and Wild-Type NR Proteins

	$K_m^{nitrate}$ (μM)	k_{cat} (s^{-1})	$k_{cat}/K_m^{nitrate}$ (M^{-1} s^{-1})	ref
pH 8.5				
CSO	>20000	<0.15	ND[a]	this work
CSO-2NR	1134	0.751	6.6×10^2	this work
CSO-3NR	151.1	0.377	2.4×10^3	this work
pH 7.0				
CSO	>20000	<0.10	ND[a]	this work
CSO-2NR	445	0.65	1.4×10^3	this work
CSO-3NR	72.7	0.96	1.3×10^4	this work
S. oleracea	12	180	1.5×10^7	39
A. thaliana	90	100	1.1×10^6	24
P. pastoris	30	159	5.3×10^6	38

[a]Not determined.

Chicken SO Y322F/R450M/R452 M (3NR) Variant. While the results for the double variants of SO were intriguing, the rate of catalysis was very slow and the Michaelis constant of the enzyme was considerably higher than that of native NR enzymes. On the basis of the results of the double mutant, the active sites of NR and SO were re-evaluated, and an additional Met residue was identified as potentially being involved in catalysis as this residue changed conformation depending on the presence of sulfate in NR similar to Arg 450 in SO; additionally, this Met residue is conserved in native NR enzymes and aligned with a Val residue in SO (Figure 6). This Val residue in SO was mutated to Met to create an SO triple mutant Y322N/R450M/V452M (CSO-3NR). This CSO-3NR variant behaved like wild-type CSO during purification.[9] The CSO-3NR variant exhibited weakened ability to oxidize sulfite at pH 8.5 with a $K_m^{sulfite}$ of 6750 μM and a $k_{cat}^{sulfite}$ of −4.1 s^{-1} for a $k_{cat}/K_m^{sulfite}$ of 6.07×10^2. At pH 7.0, the variant had a $K_m^{sulfite}$ of 570 μM and a $k_{cat}^{sulfite}$ of 2.18 s^{-1} for a $k_{cat}/K_m^{sulfite}$ of

dx.doi.org/10.1021/bi201206v | *Biochemistry* 2012, 51, 1134−1147

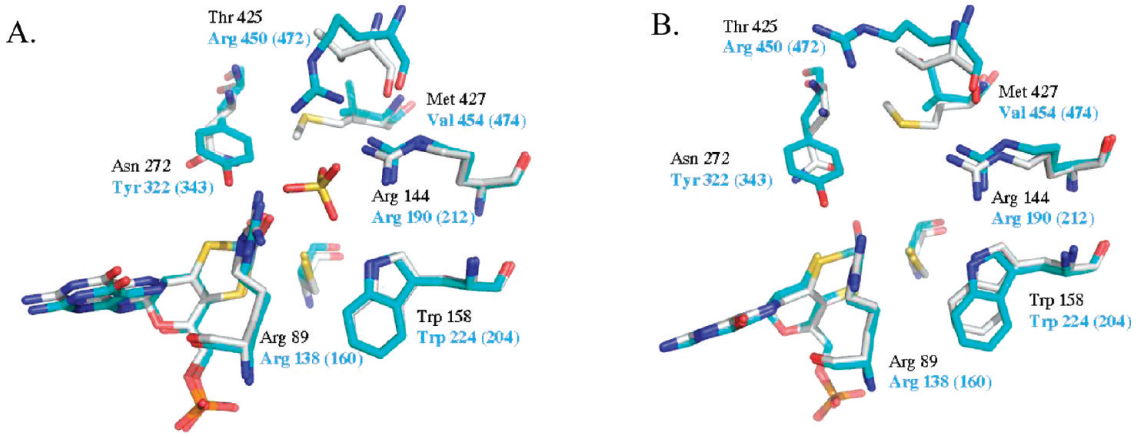

Figure 6. Overlay of yeast NR (black) and chicken SO (blue) active sites in the presence (A) and absence (B) of sulfate.

3.82×10^3 (Table 10). When assayed for nitrate reductase activity at pH 7.0, CSO-3NR exhibited a $K_m^{nitrate}$ of 72.7 μM, which is close to the $K_m^{nitrate}$ observed for native NR proteins, but a $k_{cat}^{nitrate}$ of 0.96 s^{-1} for a $k_{cat}/K_m^{sulfite}$ of 1.32×10^4, which is relatively low (Table 11).

Crystallographic Studies of Chicken 2NR and 3NR Variants via the Determination of Structures. The structures of CSO-2NR and CSO-3NR variants were determined by molecular replacement (Figure 7). The first attempt to determine the structure of CSO-2NR used the coordinates from the full-length natively purified CSO (PDB entry 1SOX), as a search model, in PHASER. Unfortunately, this approach did not yield a search solution with all components. We then used the wild-type rCSO coordinates (PDB entry 2a99 for chain A monomer residues 95−466) as the search model. Despite the fact that the full-length proteins were used for crystallization and the crystals exhibited the characteristic red color of the heme prosthetic group, no electron density was observed for the N-terminal b_5-type cytochrome domain in any of the structures we obtained, presumably because of the heme domain adopting multiple stable orientations within the crystal. These results were consistent with previously published results.[20] Both CSO-2NR and CSO-3NR crystallized in the space group $I4_1$, and all crystals had one monomer in the asymmetric unit as calculated by the Matthews coefficient.[40] Attempts were made to obtain a substrate-bound crystal of both CSO-2NR and CSO-3NR by soaking and cocrystallizing with nitrate at 1 mM, but data sets collected from both methods indicated the absence of substrate in the active site (Figure 7). This result is consistent with previously published results for the crystallization of the central Moco catalytic fragment of *P. angusta* NR.[25] The structures of CSO-2NR and CSO-3NR had good stereochemistry with all residues in the most favored and additionally allowed regions of the Ramachandran plot as determined by MOLPROBITY.[36] After several cycles of least-squares minimization and model building, the resulting crystallographic values R_{cryst} and R_{free} are reported in Table 12.

Comparison of the Crystal Structures of CSO-2NR and Wild-Type CSO. The structure of CSO-2NR was refined to 2.4 Å resolution with an R_{cryst} of 16.7 and an R_{free} of 20.7. The topology of the 2NR variant is very similar to that of the natively purified enzyme, consisting of the central Moco domain and the C-terminal dimerization domain as indicated by an rmsd of 0.142 Å for backbone atoms. As reported previously, the overall topology of the enzyme is a unique mixed $\alpha\beta$ fold.[11,20] The structure was determined by molecular replacement without solvent or cofactor atoms in the search model. A large difference density peak was observed in the active site of the enzyme that was determined to be the cofactor. The Moco was then modeled into the structure and found to be in good agreement with the density. The Moco is in a position virtually identical to that of the wild-type cofactor and bound deep inside the core of the domain held by an extensive network of hydrogen bonds and van der Waals interactions within the Moco binding pocket. The observed bond length from the Mo to the axial oxygen was 1.72 Å, and the equatorial oxygen bond distance was ~1.98 Å. The bond distance of the equatorial oxygen ligand is between the values from the previously conducted EXAFS studies that indicated a single-bond distance of 2.27 Å for the reduced molybdenum and a distance from the double-bonded oxygen to molybdenum of ~1.7 Å.[15,41,42] This suggests a partially reduced form of the molybdenum to Mo^V species. It is possible that the molybdenum of the cofactor is partially reduced either by the cryoprotectant glycerol or by photoreduction while in the synchrotron X-ray beam;[11] however, at a resolution of 2.4 Å, it is difficult to assign the exact oxidation state of the molybdenum solely on the basis of crystallographic data. Comparison of the active site residues of CSO-2NR to those of wild-type CSO indicates that several active site residues adopt conformations similar to those of residues of wild-type SO. An overlay of the two active sites reveals an rmsd of 0.091 Å between the residues of the wild type and the 2NR variant, and it is apparent that in the 2NR variant the active site residues Arg 138, Cys 185, Arg 190, and Trp 204 all adopt conformations virtually identical to those in wild-type SO (Figure 8A), indicating that these residues were not rearranged in the 2NR variant. The Asn 322 mutation's side chain appears to have moved closer to the Moco than the Tyr 322 found in the wild-type active site. The more polar side chain of the asparagine may have entered deeper into the active site than the predominately hydrophobic tyrosine. The Met 450 side chain found in the 2NR and 3NR variants appears to be in a more extended conformation compared to the Arg 450 side chain of wild-type CSO.

Comparison of the Crystal Structures of CSO-2NR and Wild-Type *P. angusta* NR. The structure of CSO-2NR is similar to the Mo domain structure of *P. angusta* wild-type NR[25] with an rmsd of 1.05 Å compared to the backbone atoms

dx.doi.org/10.1021/bi201206v | *Biochemistry* 2012, 51, 1134−1147

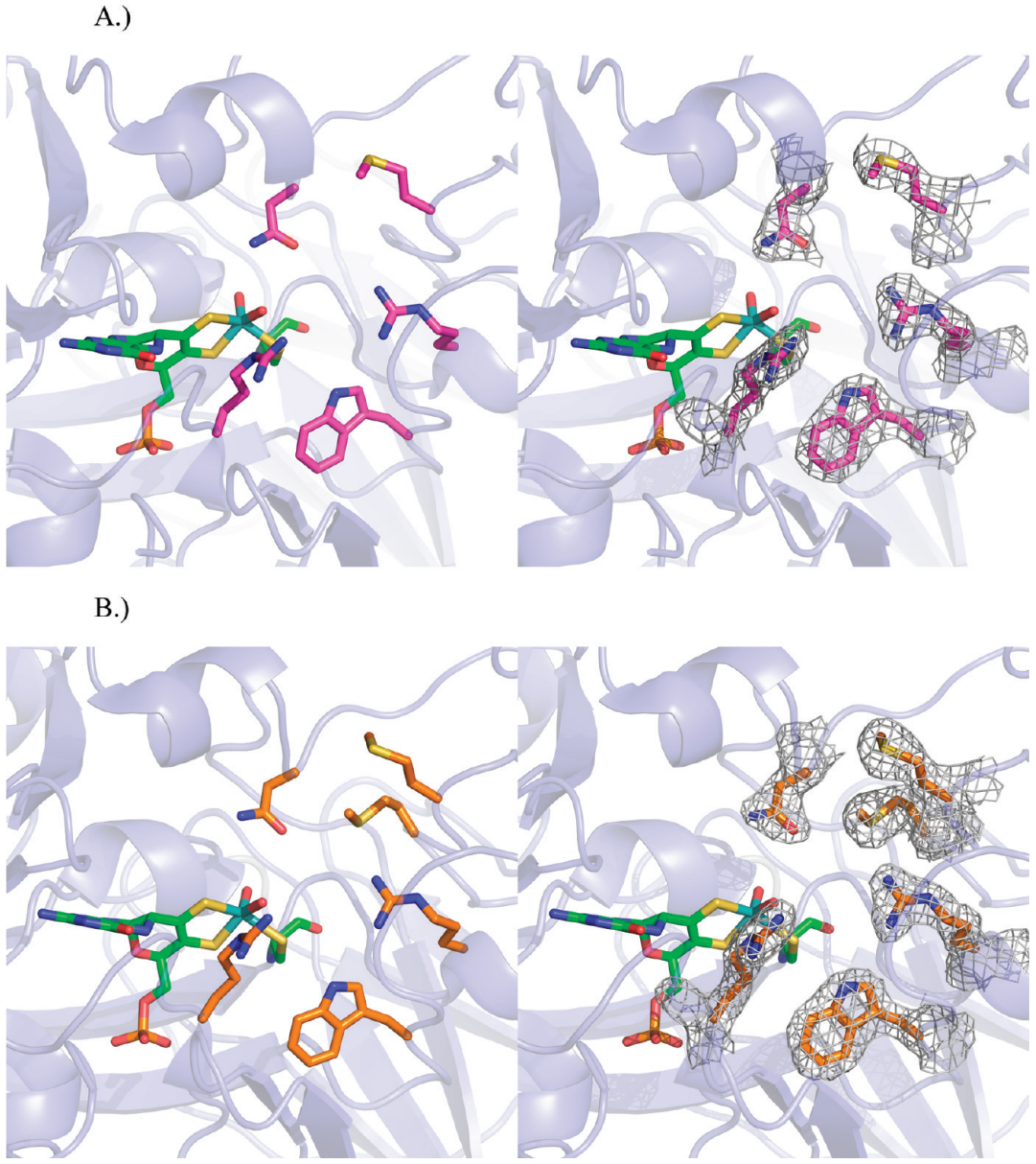

Figure 7. Structures of the active sites of (A) CSO-2NR active site residues colored magenta (left) and with electron density around active site residues (right) and (B) CSO-3NR active site residues colored orange (left) and with electron density around active site residues (right).

of NR (PDB entry 2BIH). The overall fold of the CSO-2NR variant is similar to that of *P. angusta* wild-type NR. As mentioned above, the length of the bond from the oxygen ligands of the molybdenum to the axial oxygen is 1.7 Å, and the equatorial oxygen bond distance is equal to ~1.9 Å. In the crystal structure of wild-type NR, the axial oxygen ligand of the molybdenum was at a distance of ~1.9 Å while the equatorial oxygen ligand was at a distance of ~2.1 Å, which would suggest the molybdenum of NR is in the reduced form. As NR reduces nitrate to nitrite, the enzyme is itself oxidized, so it is reasonable to suggest that the molybdenum atom of NR exists in the reduced form prior to catalysis. The distance from the oxygen ligands to the molybdenum of Moco in the 2NR structure suggests that the Mo is in an intermediate redox state. The structure of the CSO-2NR active site is similar to that of wild-type NR with an rmsd of 0.623 Å. The CSO-2NR active site residues Arg 138, Arg 190, Trp 204, and Cys 185 adopt conformations similar to those of the equivalent positions in wild-type NR (Figure 8B). The notable exception is Met 450 of CSO-2NR compared to Met 427 of wild-type NR. Met 450 of CSO-2NR is farther from the other active site residues than the wild-type Met; in addition, the side chain adopts a different orientation. In the 2NR structure, the Met 450 side chain is pointed away from the Mo atom whereas the Met side chain of *P. angusta* NR is pointed toward the Mo atom of the active site of the enzyme.

Comparison of the Crystal Structures of CSO-3NR and Wild-Type CSO. The structure of CSO-3NR was refined to 2.1 Å resolution, with an R_{cryst} of 16.9 and an R_{free} of 19.0. The structure of the 3NR variant of CSO has overall topography similar to that of wild-type SO as indicated by an rmsd of 0.121 Å for all Cα backbone atoms. A positive difference density peak was observed in the active site of the enzyme that was determined to be the cofactor. The Moco was then was modeled into the structure in good agreement with the density. The Moco of CSO-3NR is in essentially the same position as

dx.doi.org/10.1021/bi201206v | *Biochemistry* 2012, 51, 1134–1147

Table 12. Crystallographic Data and Refinement Statistics for CSO-2NR and CSO-3NR

	CSO 2NR	CSO 3NR
resolution (Å)	50−2.4	50−2.1
wavelength	1.00	1.00
space group	$I4_1$	$I4_1$
cell constants (Å)	a = 85.6	a = 85.6
	b = 85.6	b = 85.6
	c = 153.4	c = 152.8
no. of molecules per asymmetric unit	1	1
total no. of observations	102928	209711
no. of unique reflections	21499	31937
mean redundancy	4.8 (4.1)	6.6 (5.0)
R_{sym}[a] (%)	9.9 (34.5)	10.3 (28.8)
completeness (%)	99.6 (96.9)	99.7 (97.2)
mean I/σ	23.2 (3.2)	39.7 (4.3)
R_{cryt}[b] (%)	16.9	17.6
R_{free}[c] (%)	21.7	20.4
mean B factor	21.9	20.7
no. of atoms used in refinement	3084	3083
no. of waters	182	189
rmsd for bond lengths (Å)	0.013	0.011
rmsd for bond angles (deg)	1.407	1.27
Ramachandran statistics[d]	98.4/1.6	99.2/0.8

[a] $R_{sym} = \sum|I - \langle I\rangle|$, where I is the observed intensity and $\langle I\rangle$ is the average intensity of multiple symmetry-related observations of that reflection. [b] $R_{cryst} = \sum(|F_o| - |F_c|)/\sum|F_o|$, where F_o and F_c are the observed and calculated structure factors, respectively. [c] R_{free} is the R factor based on the data withheld at random from structural refinement. [d] Favored/allowed regions, with no outliers.

the Moco in the wild-type CSO enzyme. In the 3NR variant of CSO, the length of the bond from the axial oxygen ligand to the molybdenum is ∼1.70 Å and that from the equatorial oxygen is ∼2.11 Å. These bond lengths would suggest that the enzyme is closer to the reduced form of the molybdenum than the 2NR variant. This equatorial oxygen distance is closer to the single-bond hydroxyl molybdenum distance of 2.27 Å. The active site residues of CSO-3NR and wild-type CSO have adopted similar conformations as indicated by an rmsd of 0.064 Å. Inspection of the active site residues reveals that four residues (Arg 138, Arg 190, Trp 204, and Cys 185) superimposed almost perfectly between the CSO-3NR variant and the wild-type active site (Figure 9A). The Asn mutation at position 322 appears to have adopted a position similar to that of the Tyr it replaces when comparing the Cβ positions of the two side chains. The Met 450 side chain appears to be directed toward the solvent, as is Arg 450 of wild-type SO in the absence of substrate. The Met 452 mutation appears to adopt a conformation that attempts to fill the volume of the wild-type Val side chain, and the sulfur of the Met adopts a position close to the Cγ atom of the Val closest to the Moco, such that the sulfur is pointing into the active site of the enzyme.

Comparison of the Crystal Structures of CSO-3NR and Wild-Type NR. The structures of the CSO-3NR variant and the Mo domain of wild-type *P. angusta* NR (PDB entry 2BIH) share overall similarity as indicated by an rmsd of 1.08 Å when the Cα backbones are aligned. The Moco of the CSO-3NR variant is in a position virtually identical to that of the Moco of the wild-type NR structure. As discussed above, in the CSO-3NR variant, the distance from the axial oxygen ligand to the molybdenum atom is 1.7 Å and the distance from the equatorial

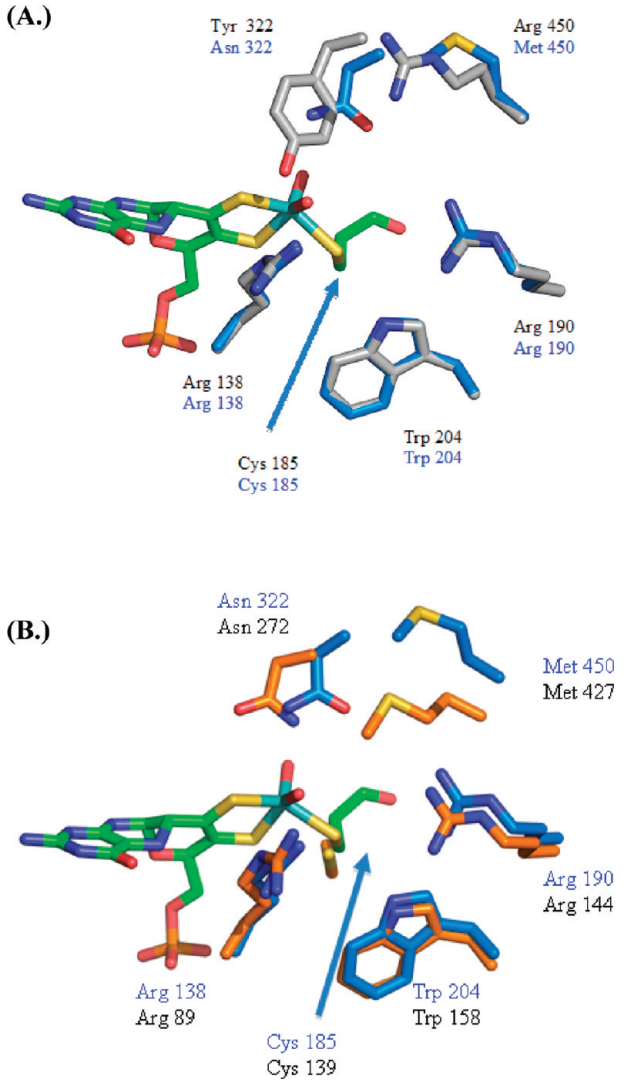

Figure 8. (A) Comparison of the active site of CSO 2NR with that of wild-type CSO colored gray and the 2NR variant colored blue. Only the Moco of 2NR is colored green. (B) Comparison of the active site of CSO 2NR with that of *P. angusta* NR colored orange and the active site of the CSO 2NR variant colored blue. Only the Moco of the 2NR is colored green.

oxygen ligand to the molybdenum is 2.1 Å. In the structure of the wild-type NR Mo domain, the distance from the axial oxygen to the molybdenum of the Moco is ∼1.98 Å and the distance from the equatorial oxygen to the molybdenum is ∼2.08 Å. As stated previously, it is possible that the molybdenum of the cofactor is partially reduced either by the cryoprotectant glycerol or by photoreduction while in the synchrotron X-ray beam.[11] The active site residues of 3NR and wild-type NR have adopted similar conformations as indicated by an rmsd of 0.658 Å. Arg 138, Cys 185, Arg 190, and Asn 322 of CSO-3NR superimpose well with Arg 89, Cys 139, Arg 144, and Asn 272 of NR, respectively. Trp 204 of CSO-3NR is in approximately the same position as Trp 158 of NR (Figure 9B). Met 450 does not align well with the Thr side chain found in a position analogous to that in wild-type NR. The Met residue at position 452 adopts an alternate conformation versus that of the wild-type Met of NR. However, the sulfur atom of Met 452 is directed into the active site and is in approximately the same position as the sulfur of the wild-type Met 427 of NR. The addition

dx.doi.org/10.1021/bi201206v | *Biochemistry* 2012, 51, 1134−1147

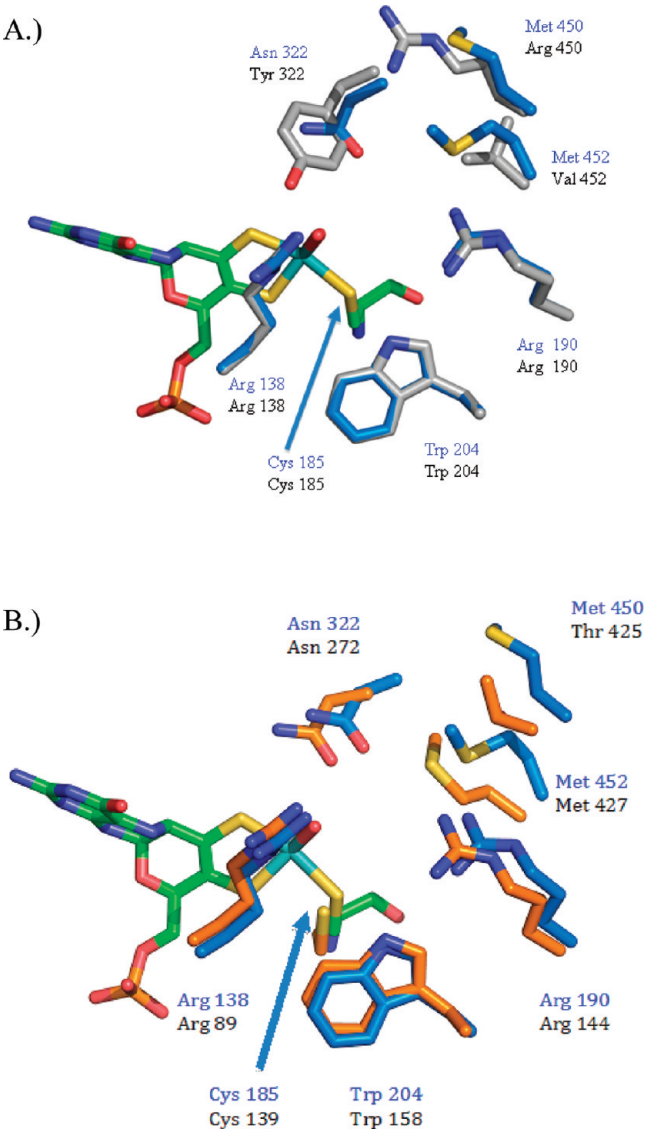

Figure 9. (A) Comparison of the active sites of CSO-3NR with wild-type CSO colored gray and the 3NR variant colored blue. Only the Moco of the 3NR is colored green. (B) Comparison of the active sites of *P. angusta* NR colored orange with the active site of the CSO 3NR variant colored blue. Only the Moco of the 3NR is colored green.

of the nonpolar Met at position 452 may also account for the Asn side chains adopting a conformation closer to that of wild-type NR than does the Asn 322 found in CSO-2NR.

Comparison of the Structures of CSO-2NR and CSO-3NR. The structures of the CSO-2NR and CSO-3NR variants are closely related as indicated by the rmsd of 0.129 Å between all aligned Cα backbone atoms. The active site Moco and residues Arg 138, Cys 185, Arg 190, and Trp 204 adopt virtually identical conformations. The additional Met substitution at position 452 appears to slightly adjust the conformation of the Asn substitution at position 322 as seen in Figure 9. The slightly larger Met appears to push the Asn side chain closer to the conformation seen in the wild-type NR active site, whereas in the 2NR variant, the Asn was further from the Moco. The additional Met 452 substitution appears to shift the conformation of the adjacent Met 450 side chain. In the structure of CSO-2NR, the sulfur of Met 450 is pointed away from the active site. In the CSO-3NR variant, Met 450 is turned around, such that the sulfur is pointed into the active site.

CONCLUSIONS

The results described in this work show that while the HSO R472Q and R472M variants have very low overall steady-state catalytic rates (Table 2), they are not significantly impaired in their ability to oxidize sulfite or to transfer electrons from Mo to the heme during the reductive half-reaction (Table 3). The mutants are much less impaired in their ability to transfer electrons to the artificial electron donor ferricyanide (Table 4). Taken together, these results provide evidence that these proteins are impaired in some aspect of the overall catalytic mechanism subsequent to the initial IET (see Figure 1).

In contrast to eukaryotic SO proteins in which the Mo and heme domains are flexibly linked and move relative to each other during the reaction cycle, a bacterial counterpart of mammalian SO, SDH from *Starkeya novella*, consists of Mo and heme domains that are products of two separate genes that are purified as a stable heterodimer.[43] Unlike mammalian SO, SDH does not undergo any conformational changes or domain movement during the catalytic cycle, and the IET rates in bacterial SDH are unaffected by altering the viscosity of the buffer solution.[44,45] In addition, the crystal structure of bacterial SDH demonstrated that the Mo and heme centers are locked in a conformation that maintains the metal centers close enough to each other to be in an IET-competent conformation throughout the catalytic cycle.[46] Superposition of the Mo domains of SDH and chicken SO shows a major difference in the orientation of the heme domains in the two enzymes. In SDH, the Mo−Fe distance is 16.6 Å, in contrast to the 32 Å separation observed in chicken SO. Furthermore, bacterial SDH lacks an arginine in the position analogous that of Arg 472 in human SO (Arg 450 in chicken SO), containing an alanine (Ala 358) instead (Figure 5). It is likely that SDH follows a different pathway for IET than mammalian SO proteins, based on the lack of domain movement during the reaction cycle.

In these studies, the native CSO proteins were mutated away from the naturally evolved SO active site sequence toward the NR active site. All the resulting single and multiple mutants were found to retain the dimeric structure but to have decreased SO activity and have gained the ability to bind and reduce nitrate to nitrite. Wild-type NR proteins can enhance the rate of nitrate reduction ($k_{cat}/K_m^{nitrate}$) by 1.5×10^7 (*S. oleracea*) to 5.3×10^6 (*P. pastoris*) times over the uncatalyzed reaction. It is remarkable that the nitrate reductase activity of CSO-3NR, with a $k_{cat}/K_m^{nitrate}$ of 1.3×10^4, is 2 orders of magnitude of greater than that of wild-type *P. pastoris* NR. The difference in $k_{cat}/K_m^{nitrate}$ between the 3NR variant is largely in part due to the lower k_{cat} for nitrate compared to those of wild-type NRs.

This study has also demonstrated that both human and chicken SO can bind and reduce nitrate with a minimum of two residues changed in the active site (HSO Y343N/R472M and CSO Y322N/R450M), and the heme domain is not necessary for full activity in the presence of a ready supply of electrons from an electron donor such as reduced methyl viologen. On the basis of both structural data and our study, Met 427 in nitrate reductase may perform a role analogous to that of Arg 472, 450, and 374 in human, chicken, and plant sulfite oxidases, respectively, in mediating conformational changes of the active site upon substrate binding. It is also possible that Met 427

dx.doi.org/10.1021/bi201206v | *Biochemistry* 2012, 51, 1134−1147

alters the redox properties of the Mo center to favor nitrate reduction.

The data presented in this paper should provide the basis for future comparative studies on SO and assimilatory NR. For instance, it would be interesting to fuse the double or triple mutant of SO to the heme and flavin domains of NR to examine whether the hybrid protein exhibits overall NADPH to nitrate activity. It would also be important to conduct detailed comparative EPR studies on NR and the several variants of SO described here, including assessment of signal shapes and relative reduction potentials.

■ ASSOCIATED CONTENT

Accession Codes

Coordinates and structure factors for CSO-2NR and CSO-3NR have been deposited in the Protein Data Bank as entries 3R18 and 3R19, respectively.

■ AUTHOR INFORMATION

Corresponding Author

*Department of Biochemistry, Box 3711, Duke University Medical Center, Durham, NC 27710. Telephone: (919) 681-8845. Fax: (919) 684-8919. E-mail: k.rajagopalan@duke.edu.

Present Address

†Division of Experimental Medicine, Harvard Medical School, Beth Israel Deaconess Medical Center, Boston, MA 02215.

Funding

This work was supported by National Institutes of Health Grant GM00091 to K.V.R.

Notes

The authors declare no competing financial interest.

■ ACKNOWLEDGMENTS

We thank Mr. Graham Alexander and Ms. Ashley Carpenter for technical assistance with cloning and protein purification.

■ ABBREVIATIONS

SO, sulfite oxidase; NR, nitrate reductase; Moco, molybdenum cofactor; MPT, molybdopterin; EXAFS, extended X-ray absorption fine structure; CEPT, coupled electron−proton transfer; IET, intramolecular electron transfer; HPLC, high-performance liquid chromatography; cyt *c*, cytochrome *c*; HSO-2NR, Y343N/R472M human SO double variant with NR activity; CSO-2NR, Y322N/R450M chicken SO double variant with NR activity; HSO-3NR, Y343N/R472M/V474M human SO triple variant with NR activity; CSO-3NR, Y322F/R450M/V452M chicken SO triple variant with NR activity; rmsd, root-mean-square deviation.

■ REFERENCES

(1) Kessler, D. L., and Rajagopalan, K. V. (1974) Hepatic sulfite oxidase. Identification of the molybdenum center as the site of irreversible inactivation by ferricyanide. *Biochim. Biophys. Acta 370*, 399−409.

(2) Johnson, J. L., Hainline, B. E., and Rajagopalan, K. V. (1980) Characterization of the molybdenum cofactor of sulfite oxidase, xanthine oxidase, and nitrate reductase. Identification of a pteridine as a structural component. *J. Biol. Chem. 255*, 1783−1786.

(3) Garrett, R. M., and Rajagopalan, K. V. (1996) Site-directed mutagenesis of recombinant sulfite oxidase: Identification of cysteine 207 as a ligand of molybdenum. *J. Biol. Chem. 271*, 7387−7391.

(4) Rupar, C. A., Gillett, J., Gordon, B. A., Ramsay, D. A., Johnson, J. L., Garrett, R. M., Rajagopalan, K. V., Jung, J. H., Bacheyie, G. S., and Sellers, A. R. (1996) Isolated sulfite oxidase deficiency. *Neuropediatrics 27*, 299−304.

(5) Shih, V. E., Abroms, I. F., Johnson, J. L., Carney, M., Mandell, R., Robb, R. M., Cloherty, J. P., and Rajagopalan, K. V. (1977) Sulfite oxidase deficiency. Biochemical and clinical investigations of a hereditary metabolic disorder in sulfur metabolism. *N. Engl. J. Med. 297*, 1022−1028.

(6) Johnson, J. L., and Rajagopalan, K. V. (1976) Human sulfite oxidase deficiency. Characterization of the molecular defect in a multicomponent system. *J. Clin. Invest. 58*, 551−556.

(7) Bailey, J. L., and Cole, R. D. (1959) Studies on the reaction of sulfite with proteins. *J. Biol. Chem. 234*, 1733−1739.

(8) Brody, M. S., and Hille, R. (1999) The kinetic behavior of chicken liver sulfite oxidase. *Biochemistry 38*, 6668−6677.

(9) Kessler, D. L., and Rajagopalan, K. V. (1972) Purification and properties of sulfite oxidase from chicken liver. Presence of molybdenum in sulfite oxidase from diverse sources. *J. Biol. Chem. 247*, 6566−6573.

(10) Johnson, J. L., and Rajagopalan, K. V. (1976) Purification and properties of sulfite oxidase from human liver. *J. Clin. Invest. 58*, 543−550.

(11) Kisker, C., Schindelin, H., Pacheco, A., Wehbi, W. A., Garrett, R. M., Rajagopalan, K. V., Enemark, J. H., and Rees, D. C. (1997) Molecular basis of sulfite oxidase deficiency from the structure of sulfite oxidase. *Cell 91*, 973−983.

(12) Qiu, J. A., Wilson, H. L., Pushie, M. J., Kisker, C., George, G. N., and Rajagopalan, K. V. (2010) The structures of the C185S and C185A mutants of sulfite oxidase reveal rearrangement of the active site. *Biochemistry 49*, 3989−4000.

(13) Feng, C., Wilson, H. L., Hurley, J. K., Hazzard, J. T., Tollin, G., Rajagopalan, K. V., and Enemark, J. H. (2003) Essential role of conserved arginine 160 in intramolecular electron transfer in human sulfite oxidase. *Biochemistry 42*, 12235−12242.

(14) Doonan, C. J., Wilson, H. L., Rajagopalan, K. V., Garrett, R. M., Bennett, B., Prince, R. C., and George, G. N. (2007) Modified Active Site Coordination in a Clinical Mutant of Sulfite Oxidase. *J. Am. Chem. Soc. 129*, 9421−9428.

(15) George, G. N., Kipke, C. A., Prince, R. C., Sunde, R. A., Enemark, J. H., and Cramer, S. P. (1989) Structure of the active site of sulfite oxidase. X-ray absorption spectroscopy of the Mo(IV), Mo(V), and Mo(VI) oxidation states. *Biochemistry 28*, 5075−5080.

(16) Pacheco, A., Hazzard, J. T., Tollin, G., and Enemark, J. H. (1999) The pH dependence of intramolecular electron transfer rates in sulfite oxidase at high and low anion concentrations. *J. Biol. Inorg. Chem. 4*, 390−401.

(17) Wilson, H. L., and Rajagopalan, K. V. (2004) The role of tyrosine 343 in substrate binding and catalysis by human sulfite oxidase. *J. Biol. Chem. 279*, 15105−15113.

(18) Feng, C., Wilson, H. L., Hurley, J. K., Hazzard, J. T., Tollin, G., Rajagopalan, K. V., and Enemark, J. H. (2003) Role of conserved tyrosine 343 in intramolecular electron transfer in human sulfite oxidase. *J. Biol. Chem. 278*, 2913−2920.

(19) Schrader, N., Fischer, K., Theis, K., Mendel, R. R., Schwarz, G., and Kisker, C. (2003) The crystal structure of plant sulfite oxidase provides insights into sulfite oxidation in plants and animals. *Structure 11*, 1251−1263.

(20) Karakas, E., Wilson, H. L., Graf, T. N., Xiang, S., Jaramillo-Busquets, S., Rajagopalan, K. V., and Kisker, C. (2005) Structural insights into sulfite oxidase deficiency. *J. Biol. Chem. 280*, 33506−33515.

(21) Banks, G. R., Shelton, P. A., Kanuga, N., Holden, D. W., and Spanos, A. (1993) The *Ustilago maydis* nar1 gene encoding nitrate reductase activity: Sequence and transcriptional regulation. *Gene 131*, 69−78.

(22) Johnstone, I. L., McCabe, P. C., Greaves, P., Gurr, S. J., Cole, G. E., Brow, M. A., Unkles, S. E., Clutterbuck, A. J., Kinghorn, J. R., and Innis, M. A. (1990) Isolation and characterisation of the crnA-niiA-niaD gene cluster for nitrate assimilation in *Aspergillus nidulans*. *Gene 90*, 181−192.

(23) Crawford, N. M., Smith, M., Bellissimo, D., and Davis, R. W. (1988) Sequence and nitrate regulation of the *Arabidopsis thaliana* mRNA encoding nitrate reductase, a metalloflavoprotein with three functional domains. *Proc. Natl. Acad. Sci. U.S.A. 85*, 5006−5010.
(24) Skipper, L., Campbell, W. H., Mertens, J. A., and Lowe, D. J. (2001) Pre-steady-state kinetic analysis of recombinant *Arabidopsis* NADH:nitrate reductase: Rate-limiting processes in catalysis. *J. Biol. Chem. 276*, 26995−27002.
(25) Fischer, K., Barbier, G. G., Hecht, H. J., Mendel, R. R., Campbell, W. H., and Schwarz, G. (2005) Structural basis of eukaryotic nitrate reduction: Crystal structures of the nitrate reductase active site. *Plant Cell 17*, 1167−1179.
(26) Fersht, A. R., and Winter, G. P. (1985) Redesigning enzymes by site-directed mutagenesis. *Ciba Found. Symp. 111*, 204−218.
(27) Temple, C. A., Graf, T. N., and Rajagopalan, K. V. (2000) Optimization of expression of human sulfite oxidase and its molybdenum domain. *Arch. Biochem. Biophys. 383*, 281−287.
(28) Ho, S. N., Hunt, H. D., Horton, R. M., Pullen, J. K., and Pease, L. R. (1989) Site-directed mutagenesis by overlap extension using the polymerase chain reaction. *Gene 77*, 51−59.
(29) Johnson, J. L. (1988) Molybdenum. *Methods Enzymol. 158*, 371−382.
(30) Yu, L., and Wolin, M. J. (1969) Hydrogenase measurement with photochemically reduced methyl viologen. *J. Bacteriol. 98*, 51−55.
(31) Borek, D., Minor, W., and Otwinowski, Z. (2003) Measurement errors and their consequences in protein crystallography. *Acta Crystallogr. D59*, 2031−2038.
(32) McCoy, A. J. (2007) Solving structures of protein complexes by molecular replacement with Phaser. *Acta Crystallogr. D63*, 32−41.
(33) Emsley, P., and Cowtan, K. (2004) Coot: Model-building tools for molecular graphics. *Acta Crystallogr. D60*, 2126−2132.
(34) Word, J. M., Bateman, R. C. Jr., Presley, B. K., Lovell, S. C., and Richardson, D. C. (2000) Exploring steric constraints on protein mutations using MAGE/PROBE. *Protein Sci. 9*, 2251−2259.
(35) Murshudov, G. N., Vagin, A. A., and Dodson, E. J. (1997) Refinement of macromolecular structures by the maximum-likelihood method. *Acta Crystallogr. D53*, 240−255.
(36) Davis, I. W., Leaver-Fay, A., Chen, V. B., Block, J. N., Kapral, G. J., Wang, X., Murray, L. W., Arendall, W. B. III, Snoeyink, J., Richardson, J. S., and Richardson, D. C. (2007) MolProbity: All-atom contacts and structure validation for proteins and nucleic acids. *Nucleic Acids Res. 35*, W375−W383.
(37) Painter, J., and Merritt, E. A. (2006) Optimal description of a protein structure in terms of multiple groups undergoing TLS motion. *Acta Crystallogr. D62*, 439−450.
(38) Barbier, G. G., Joshi, R. C., Campbell, E. R., and Campbell, W. H. (2004) Purification and biochemical characterization of simplified eukaryotic nitrate reductase expressed in *Pichia pastoris*. *Protein Expression Purif. 37*, 61−71.
(39) Pollock, V. V., Conover, R. C., Johnson, M. K., and Barber, M. J. (2002) Bacterial expression of the molybdenum domain of assimilatory nitrate reductase: Production of both the functional molybdenum-containing domain and the nonfunctional tungsten analog. *Arch. Biochem. Biophys. 403*, 237−248.
(40) Matthews, B. W. (1968) Solvent content of protein crystals. *J. Mol. Biol. 33*, 491−497.
(41) Cramer, S. P., Wahl, R., and Rajagopalan, K. V. (1981) Molybdenum sites of sulfite oxidase and xanthine dehydrogenase. A comparison by EXAFS. *J. Am. Chem. Soc. 103*, 7721−7727.
(42) Harris, H. H., George, G. N., and Rajagopalan, K. V. (2006) High-resolution EXAFS of the active site of human sulfite oxidase: Comparison with density functional theory and X-ray crystallographic results. *Inorg. Chem. 45*, 493−495.
(43) Kappler, U., Friedrich, C. G., Truper, H. G., and Dahl, C. (2001) Evidence for two pathways of thiosulfate oxidation in *Starkeya novella* (formerly *Thiobacillus novellus*). *Arch. Microbiol. 175*, 102−111.
(44) Feng, C., Kedia, R. V., Hazzard, J. T., Hurley, J. K., Tollin, G., and Enemark, J. H. (2002) Effect of solution viscosity on intramolecular electron transfer in sulfite oxidase. *Biochemistry 41*, 5816−5821.
(45) Feng, C., Kappler, U., Tollin, G., and Enemark, J. H. (2003) Intramolecular electron transfer in a bacterial sulfite dehydrogenase. *J. Am. Chem. Soc. 125*, 14696−14697.
(46) Kappler, U., and Bailey, S. (2005) Molecular basis of intramolecular electron transfer in sulfite-oxidizing enzymes is revealed by high resolution structure of a heterodimeric complex of the catalytic molybdopterin subunit and a c-type cytochrome subunit. *J. Biol. Chem. 280*, 24999−25007.